Published in final edited form as:

NMR Biomed. 2020 February ; 33(2): e4217. doi:10.1002/nbm.4217.

R1ρ Sensitivity to pH and Other Compounds at Clinically Accessible Spin-Lock Fields in the Presence of Proteins

Nana Owusu[1,3], **Casey P. Johnson**[4], **William Kearney**[1], **Dan Thedens**[1], **John Wemmie**[2], **Vincent A. Magnotta**[1,2,3]

[1]Department of Radiology, University of Iowa, Iowa City, IA, USA

[2]Department of Psychiatry, University of Iowa, Iowa City, IA, USA

[3]Department of Biomedical Engineering, University of Iowa, Iowa City, IA, USA

[4]Center for Magnetic Resonance Research, University of Minnesota, Minneapolis, MN, USA

Abstract

Numerous human diseases involve abnormal metabolism, and proton exchange is an effective source of magnetic resonance imaging (MRI) contrast for assessing metabolism. One MRI technique that capitalizes on proton exchange is R_1 relaxation in the rotating frame ($R_{1\rho}$). Here we investigated the sensitivity of $R_{1\rho}$ to various proton-exchange mechanisms at spin-lock pulses within FDA safety guidelines for radiofrequency-induced heating. We systematically varied pH known to change the rate of proton exchange as well as the glucose and lysine concentrations, thus changing the number of amide, hydroxyl, and amine exchangeable sites in a series of egg-white albumin phantoms. The resulting effects on quantitative relaxation time measurements of $R_{1\rho}$, R_1, and R_2 were observed at 3T. Using spin-lock amplitudes available for human imaging (less than 23.5μT) at near physiologic temperatures, we found $R_{1\rho}$ was more sensitive to physiologic changes in pH than to changes in glucose and lysine concentrations. In addition, $R_{1\rho}$ was more sensitive to pH changes than R_1 and R_2. Models of proton exchange fit to the relaxation measurements suggest that amide groups were the primary source of pH sensitivity. Together, these experiments suggest an optimal spin-lock amplitude for measuring pH changes while not exceeding FDA subject heating limitations.

Keywords

Multi-parametric imaging; $R_{1\rho}$ dispersion; physical phantom; temperature; glucose; lysine; pH

Corresponding Author: Vincent A. Magnotta; vincent-magnotta@uiowa.edu.

AUTHORS' CONTRIBUTION

NO conducted all the imaging experiments and produced all the figures, WK and NO produced the values from two-pool model results. NO, VAM, and WK interpreted the data. CJ and DT modified imaging sequences for adiabatic excitation. NO and VAM prepared the manuscript with input from CJ, WK, and JW. All authors read and approved the final manuscript.

ADDITIONAL INFORMATION

The authors declare that they have no competing interests.

$R_{1\rho}$ sensitivity to different exchange rates at clinically accessible ($B_0 \leq 3T$) field strengths is not well characterized and this work is to address that question for 3T. Multiparametric mapping of three phantoms with gradations of metabolite concentrations and pH values shows $R_{1\rho}$ sensitivity to physiologic pH range in protein solutions at 3T. Modeling of proton exchange with relaxation measures suggests amide proton exchange is the likely source of pH sensitivity.

INTRODUCTION

Proton exchange is being increasingly utilized as a source of intrinsic contrast in magnetic resonance imaging (MRI). In tissue, water protons are continuously exchanged with protons on amide (O=C-NH-), hydroxyl (-OH) and amine ($-NH_2$) groups abundant in macromolecules such as proteins. The magnetization of protons in water and macromolecules is sensitive to this exchange. The rate of exchange (k_{ex}) depends on the forward (k_1) and reverse (k_{-1}) rate constants and can range from 10–500s^{-1} for amide protons to 500–10,000s^{-1} for hydroxyl and amine protons[1].

$$k_{ex} = k_1 + k_{-1}. \quad (1)$$

The two most commonly used MRI techniques sensitive to proton exchange are R_1 relaxation in the rotating frame ($R_{1\rho}$) and chemical exchange saturation transfer (CEST). These techniques have been used to study several psychiatric and neurological disorders including Alzheimer's Disease[2–4], Parkinson's Disease [5], Huntington's Disease [6], panic disorder [7], and bipolar disorder [8,9]. Both static[8,9] and functional[7] changes in $R_{1\rho}$ relaxation rates have been observed, which have been interpreted to be driven at least in part by abnormalities in brain pH. However, solvent concentrations or other macromolecules could also contribute to the observed changes. Relatively little work has been done to characterize $R_{1\rho}$ relaxation rates using commonly employed clinical MRI field strengths (e.g. 3T) and spin-lock amplitudes that are within the Food and Drug Administration (FDA) radiofrequency heating limits.

MRI pulse sequences for acquiring $R_{1\rho}$ typically involve a spin-lock block comprised of the following: 1) a 90° radiofrequency (RF) pulse tipping the magnetization into the transverse plane; 2) a spin-lock RF pulse of constant amplitude; and 3) a second 90° RF pulse restoring the magnetization to the longitudinal direction[10]. To help minimize B_1 and B_0 sensitivity of the spin-lock block, adiabatic 90° RF pulses can be used[11], and the phase of the spin-lock pulse can be alternated for each half of its duration[12]. $R_{1\rho}$ relaxation rate can be calculated from two or more images with different spin-lock pulse durations (TSL) using Equation 2:

$$R_{1\rho} = \frac{1}{T_{1\rho}} = -\ln\left(\frac{S_{TSL}}{S_0}\right)/TSL, \quad (2)$$

where S_{TSL} is the signal collected after applying the spin-lock block and S_0 is the signal without applying the spin-lock pulse. Previous work has attributed the sensitivity at lower spin-lock amplitudes to amide exchange and other low frequency processes[13,14] while work at ultra-high magnetic fields and large spin-lock amplitudes (greater than 23.5μT) have found that spin-lock pulses are sensitive to hydroxyl and amine protons[15,16].

While a number of studies have aimed to discern factors affecting $R_{1\rho}$ relaxation rates, these studies have almost exclusively been conducted with high spin-lock amplitudes greater than 23.5μT (equivalent to a frequency of more than 1000 Hz) and/or using ultrahigh-field (7T or higher) small bore scanners where specimen heating was not a concern or was not monitored[17–19]. Such studies have identified a number of important factors[20] contributing to

$R_{1\rho}$ relaxation rates including solute concentration (glucose[21] and glutamate[17]), pH[22], temperature[23] and molecular rotational rate[24]. Other contributions to $R_{1\rho}$ relaxation rates have been identified including interactions between large macromolecules and water via dipolar and diffusion relaxation pathways[25,26]. Moreover, outcomes from $R_{1\rho}$ relaxation rate studies depended on both field strength[27] and the amplitude of the applied spin-lock pulse[28]. To better understand the contributions from several sources including proton exchange, diffusion, temperature, and pH Spear and Gore recently undertook an extensive study to explore their effect on $R_{1\rho}$ relaxation rates[29]. They showed that temperature and pH were two key factors that influenced the rate of proton exchange. In addition, they showed that the multiple pools of exchanging protons behave independently and that multiple R1ρ measurements can be used to derive an exchange rate constant.

The goal of this work was to better understand the role of proton exchange with compounds abundant in brain tissue and thought to potentially contribute to $R_{1\rho}$ changes by building upon the fundamental framework of Spear and Gore. These studies may be helpful in understanding the findings previously observed in prior human studies at 3T that have identified differences in $R_{1\rho}$ relaxation times between individuals with psychiatric and neurological disorders and controls. Using well-controlled phantoms, three experiments were performed to investigate the effects of changing the chemical environment in the presence of proteins on $R_{1\rho}$ relaxation rates. This was done by adjusting pH (known to alter rate of amide proton transfer) within the phantom as well as changing the number of amide, hydroxyl, and amine exchangeable sites by adding glucose and lysine in the physiological range of concentration. These studies were performed in a 3T MRI scanner across a range of temperatures (9–34°C) while maintaining the specific absorption rate (SAR) levels within allowed FDA levels. Based on our previous $R_{1\rho}$ imaging work in phantoms and animals[30], we hypothesized that at 3T $R_{1\rho}$ would exhibit a greater sensitivity to pH as compared to the other metabolites studied.

MATERIALS & METHODS

Phantom Preparation

Phantoms were created that allowed for the systematic variation of pH, glucose, and lysine concentrations while controlling temperature. The spherical shell of a Magphan® EMR051 phantom (The Phantom Laboratory; Greenwich, NY) was used for this study. The interior of each phantom housed three fiberglass plates that were printed to hold seven 50mL Falcon tubes inside the sphere. The plugs at either end of the phantom were replaced with nylon barbs used to connect tygon tubing to the phantom providing a constant temperature water bath to the tubes inside the phantom. The other end of the hoses was connected to a water recirculating system (Endocal RTE-110, NESLAB) housed outside of the scan room (Supplementary Materials, Figure S1).

Experiments were performed using four separate phantoms, which contained various concentrations of pH, glucose, lysine, and water (control) added to 45 mL liquid egg-white albumin (HyVee generic brand, 0.124mM of proteins). The first phantom tested the effects of pH on $R_{1\rho}$. Varying amounts of hydrochloric acid (HCl, 1N) were added to different Falcon tubes to produce pH values across a physiologically relevant range (pH 6.01, 6.51,

7.02, 7.25, 7.51, 7.79 and 8.0). pH was confirmed using an Accumet *AB15* pH meter (Fisher Scientific; Pittsburg, PA). The second phantom tested the effects of changing the concentration of hydroxyl exchange sites by changing glucose concentration. Glucose concentration was varied from 0, 5, 10, 15, 20, 30, and 40 mM (pH 9.03 for all vials). The third phantom tested the effects of changing the number of amine exchange sites. Lysine concentration was varied from 0, 0.5, 1.0, 1.5, 2.0, 2.5, and 3.0 mM (pH 9.03 for all vials). The pH, glucose, and lysine concentrations were selected to encompass the physiological range expected in the *in vivo* brain. The first three phantoms allowed for the exploration of proton exchange mediated by changing the rate of exchange versus changes in the number of exchangeable sites. The fourth phantom was a water control phantom that contained two sets of three vials diluted with either water or HCl (1N) (1, 2, and 3mL). The seventh vial contained only liquid egg whites. pH was then measured in the tubes, and the pH for the water-containing vials was 9.03, 9.04, and 9.05 while the HCl-containing vials had pH values of 7.42, 6.46 and 5.93, respectively. The tube containing only egg whites had a pH of 9.00.

MR Imaging

All MR imaging was performed on a Siemens 3T TIM Trio MRI scanner (Erlangen, Germany). The spherical phantom was placed in a circularly polarized head coil. The thermostatic bath was then set to the appropriate temperature (9, 22, 34°C) for the imaging experiment and allowed to circulate for 30 minutes before initiating imaging. Temperature within the phantom was measured at the start and end of each imaging experiment. Imaging included a three-plane localizer, B_0 mapping, B_1 mapping, and $R_{1\rho}$, R_2, and R_1 relaxation rate mapping. $R_{1\rho}$ mapping was collected in the coronal plane using a continuous-wave spin-lock preparation pulse and adiabatic excitation in a turbo spin-echo sequence with the following parameters: TR = 5000 ms, TE = 12 ms, slice thickness = 5.0 mm, FOV = 22.0×22.0 cm, matrix = 256×256, bandwidth = 130 Hz/pixel, time of spin-lock (TSL) = 0 and 100 ms, turbo factor = 4. Johnson *et al.* have shown that optimal SNR can be achieved with two spin-lock times[31], thus the spin-lock times here were chosen while maintaining SAR within FDA limits. At room temperature, the egg-white medium had an $R_{1\rho}$ of 3.92. R_2 mapping was acquired using Malcom-Levitt (MLEV) preparation with four refocusing hard pulses, which provided effective echo times of 0 and 100 ms. All other imaging parameters were the same as the $R_{1\rho}$ based turbo spin-echo sequence. R_1 mapping was collected using a coronal inversion recovery (IR) sequence with the following parameters: TR = 5000 ms, TE = 12 ms, slice thickness = 5.0 mm, FOV = 22.0×22.0 cm, matrix = 256×256, Bandwidth = 130 Hz/pixel. Sequential acquisitions were performed with TI = 50, 150, 250, 450, 750, and 1150 ms. Three separate measurements were obtained for $R_{1\rho}$, R_2 and R_1 in each phantom preparation and temperature with different vial placements for each measurement.

For the pH, glucose, and lysine phantoms, $R_{1\rho}$ imaging was performed at four spin-lock field strengths (4.7, 9.4, 14.1, and 18.8μT) corresponding to frequencies of 200, 400, 600 and 800 Hz to assess sensitivity across a variety of spin-lock amplitudes that may be applied *in vivo*. These phantoms were imaged at 9, 22, and 34°C. The water control phantom was assessed using only the 9.4μT spin-lock pulse at 22°C.

MR Image Analysis

To generate the relaxation maps, voxel-by-voxel calculation of the relaxation rates was performed using MATLAB (MathWorks; Natick, MA). $R_{1\rho}$ and R_2 were calculated by fitting the respective TSL or TE to a single exponential decay model (Eq. 2), and R_1 was calculated using a single exponential recovery model as specified in Equation 3.

$$R_1 = \frac{1}{T_1} = -\ln\left(\left(S_0 - S_{TI}\right)/2S_0\right)/TI \tag{3}$$

Once the relaxation maps were generated, regions of interest (ROI) were manually defined for each tube in MATLAB (Fig. 3). The resulting ROIs were placed in regions where the B_0 field map was between 0.5–1.2Hz and the B_1 map was between ±10°. The median value and standard deviation were obtained from each ROI. This was done independently for each of the repeated measurements, relaxation property, and phantom preparations. This allowed us to evaluate both the sensitivity as well as the reliability of the measurements. To visualize the results, the plots were normalized to one of the metabolite concentrations. The relaxation parameters were normalized to the results obtained at 7.02 (pH), 15mM (glucose), and 1.5mM (lysine), respectively. The change in the relaxation rates relative to these reference concentrations were plotted as percent changes. Error propagation was used to translate the standard deviation at each vial onto the percentage change plots.

Circular Dichroism Experiment—To determine if the proteins in the pH phantom were denatured as result of adding HCl to the egg white albumin, circular dichroism measurements were obtained. Eleven vials (50mL) were produced with egg white albumin, phosphate buffered saline solutions at pH ranging from 6 to 8 with steps of 0.2 by doping the solutions with HCl and sodium hydroxide (NaOH). At temperatures similar to those used in the imaging experiments (4, 22, 37°C), circular dichroism spectra were obtained in the samples at wavelengths 190–260. These measurements were repeated 5 times. A ratio of absorbance at 222 and 208nm was used to assess if changes in protein folding were observed[32].

Two-Pool Model Fit to Relaxation Measurements—To estimate the type of solute protons responsible for the pH sensitivity of the $R_{1\rho}$ measurements, a two-pool proton exchange model, based on the work of Chopra *et al.*[27] and adapted by Cobb *et al.*[33,34], was fit to the $R_{1\rho}$ relaxation measurements. This model describes $R_{1\rho}$ for protons undergoing two-site exchange as follows [29,35]:

$$R_{1\rho} = \frac{1}{T_{1\rho}} = \frac{R_2 S_p^2 + R_{1\rho}^{\infty}\omega_1^2}{S_p^2 + \omega_1^2}; S_p^2 = \frac{R_{1b} + r_b}{R_{2b} + r_b}((R_{2b} + r_b)^2 + \Delta\omega_b^2)\,. \tag{4}$$

In Equation 4, R_2 is the transverse relaxation rate for the system and $R_{1\rho}{}^{\infty}$ is the value of $R_{1\rho}$ when then spin lock amplitude approaches infinity. R_{1b} ($=1/T_{1b}$) and R_{2b} ($=1/T_{2b}$) are the longitudinal and transverse relaxation rates of bound protons in the laboratory frame. The proton exchange rate is r_b and $\Delta\omega_b$ is the chemical-shift of the solute protons (from the water frequency) while ω_1 is the applied spin-lock amplitude.

For each pH value, Equation 4 was fit to the experimental $R_{1\rho}$ measurements as a function of the applied spin-lock amplitude, with $\Delta\omega_b$ and r_b set to values appropriate for exchange with amide protons ($\Delta\omega_b$ =3.35ppm, r_b =20s^{-1})[36], hydroxyl groups ($\Delta\omega_b$ =1.25ppm, r_b =1500s^{-1})[36], and amines ($\Delta\omega_b$ =3ppm, r_b =4000s^{-1})[36]. The relaxation rates of amide protons (R_{1b} = 0.51 s^{-1} and R_{2b} = 4.19 s^{-1}), glucose (R_{1b} = 0.20 s^{-1} and R_{2b}= 0.50 s^{-1}), and lysine (R_{1b} = 0.50 s^{-1} and R_{2b} = 1.00 s^{-1}) as measured by Sykes et al. for ovalbumin at B_0=100MHz (2.35T)[37] were used. The fitnlm function in MATLAB was then used to generate a non-linear fit of Equation 4 to the R1ρ dispersion measurements at each pH, solving for $R_{1\rho}^{\infty}$, R_2, and r_b. The values specified above for r_b was used as an initial condition for the fitting procedure while initial values were assigned to R_2 and $R_{1\rho}^{\infty}$ based on the R_2 and R_1 relaxation rates observed in the MR imaging experiments. These values were just initial conditions and the parameters were then allowed to float during model fitting. The resulting estimates for the relaxation rates were compared to those obtained experimentally.

RESULTS

Example $R_{1\rho}$ relaxation rate maps obtained in the pH, glucose, and lysine phantoms are shown in Figure S2 of the Supplementary Materials. ROI based measurements obtained from these maps for $R_{1\rho}$, R_2, and R_1 relaxation rates are summarized below. Examples of the B_0 maps are shown in Figure S3 of the Supplementary Materials.

pH Phantom

$R_{1\rho}$ mapping of the pH phantom showed the expected sensitivity to pH. Relaxation rate percent change plots for $R_{1\rho}$ with 400Hz spin-lock amplitude are shown in Figure 1a. The sensitivity to pH was observed across the entire experimental temperature range and at 34°C $R_{1\rho}$ showed the greatest sensitivity to pH changes as compared to R_2 and R_1 relaxation. Changes in $R_{1\rho}$ relaxation rates did show a subtle dependence on temperature with a larger decrease observed at 9°C (approx. −30%) as compared to 34°C (approx. −25%) across the pH range studied (6.0–8.0). The $R_{1\rho}$ relaxation rates ranged from 2.18 to 3.7 s^{-1} at 9°C and from 2.41 to 3.4 s^{-1} at 34°C. Little difference was observed between the $R_{1\rho}$ relaxation rates at 34°C and 22°C. In the water control phantom, small changes in the water concentration did not change the $R_{1\rho}$ relaxation rates (Supplementary Materials Figure S4).

R_2 relaxation rates were sensitive to pH in the phantom similar to those observed for $R_{1\rho}$ relaxation rates (Figure 1b). However, the R_2 experiments showed a greater temperature dependence. A 35% decrease in R_2 relaxation rates at pH 6.0 relative to pH 7.02 was observed at 9°C, which as reduced to 12% at 34°C. Only small variations (approx. 5%) in the R_2 relaxation rates were observed above pH 7.0. Figure S5b in the Supplementary Materials shows the temperature sensitivity for the R_2 measurements.

The R_1 relaxation rates showed very little sensitivity to pH with decreases of less than 10% between pH 6.0 and 7.0 (Figure 1c). In addition, the pH sensitivity did not change with temperature.

Glucose Phantom

By adding varying concentrations of glucose to liquid egg-white solutions, the number of hydroxyl exchangeable sites was increased. Figure 1 shows the relative change plots of the relaxation rates acquired with respect to temperature. $R_{1\rho}$ relaxation rates showed very little change in response to glucose concentration at three temperatures studied (Figure 1d). Across the glucose concentration range studied in this experiment, $R_{1\rho}$ relaxation rates showed changes of 6%, 4%, and 5% at 9, 22, and 34°C respectively. Similar small changes were observed for R_2 (Figure 1e) and R_1 (Figure 1f) relaxation rates in the phantom at 34°C. At lower temperatures, variation in the R_2 relaxation rates were observed between the tubes containing 0 and 5mM concentrations of glucose, but little change was observed between 5 and 40 mM.

Lysine Phantom

Fast exchanging amine protons were added to liquid egg-white solutions by adding lysine at varying concentrations. All three of the quantitative relaxation measures ($R_{1\rho}$, R_2, and R_1) showed little sensitivity to the lysine concentrations added to the various tubes in the phantom (Figure 1, g–i). $R_{1\rho}$ showed had 4% change across the full concentration range used in this study at 34°C.

Dispersion Data

The impact of the $R_{1\rho}$ spin-lock pulse amplitude was also explored in this study. The overall RF energy deposited in the body is limited by the FDA and practically, this limits the maximum amplitude of the spin-lock pulse to be 1000Hz or less to keep the RF levels below the FDA limit in a clinically acceptable acquisition time. The sensitivity of $R_{1\rho}$ to changes in pH, glucose, and lysine concentrations was evaluated for spin-lock amplitudes ranging from 4.7 to 18.8 μT (200–800Hz) to determine if the sequence was sensitive to different exchange rates based on the amplitude of the spin-lock pulse. In Figure 2 the relative changes in R1ρ relaxation rates are shown for each phantom at 34°C. For $R_{1\rho}$, the 18.8 μT (800Hz) spin-lock produced the greatest change (approx. 43%) in $R_{1\rho}$ from pH 7.01 to 6.01. The other spin-lock amplitudes also showed pH sensitivity but with a smaller change of 40% (14.2 μT), 35% (9.4 μT) and 20% (4.7 μT). $R_{1\rho}$ relaxation rates showed no sensitivity to glucose and lysine in the phantoms across all the spin-lock amplitudes used in this study.

Circular Dichroism Measurements

To discern the mechanism underlying the sensitivity of $R_{1\rho}$ imaging to pH, circular dichroism measurements were obtained. Figure 3 shows the absorbance ratio 222nm/208nm as a function of pH at 37°C. Across the pH range, there was only a slight variance in the absorption at 222nm when compared with the 208 nm reference wavelength. This means the absorption by the helical structures remained constant throughout the experiments. Thus, there was little or no denaturation of the proteins, suggesting the pH sensitivity of $R_{1\rho}$ is not likely due to changes in protein conformation.

Two-Pool Model Fit to Relaxation Measurements

To evaluate the type of exchange processes contributing to the observed $R_{1\rho}$ changes, the two-pool model described in Equation 4 was fit using parameters for amide protons, hydroxyl groups, and amines. The model behavior was only reasonable for the parameters associated with amide exchange. The model for amide exchange generated similar trends for the R_2 measurements as observed in the phantom (Table 1). Table 1 also includes the R_2 and R_1 relaxation rates measured from the imaging experiments for comparison. An error of approximately 8% was observed for the R_2 values generated from the model as compared to the experimental results. Measured $R_{1\rho}$ values were consistently between measured R_2 and calculated $R_{1\rho}^{\infty}$ for the same conditions. The model fit for the $R_{1\rho}^{\infty}$ measurements were approximately a factor of 4 shorter than the observed R_1 values in the phantom. The model behavior for parameters suitable for amines and hydroxyl groups generated unrealistic values for the fitted parameters (i.e. $R_{1\rho}^{\infty} < 0$, or extremely large r_b) and thus the corresponding models were considered to be invalid.

DISCUSSION

We have previously observed $R_{1\rho}$ relaxation rate changes in studies of psychiatric[7–9] and neurological disorders[2,5,6], which were interpreted as likely due to changes in brain pH and metabolism. This study was undertaken to better understand factors that may influence $R_{1\rho}$ relaxation rates including pH, other solutes (glucose and lysine), as well as temperature. Since the manipulation of a single compound *in vivo* is challenging, this study used a physical phantom to systematically vary compound concentrations. Imaging was performed on a 3T MRI scanner while using spin-lock amplitudes within FDA SAR limits. The key findings from the experiments showed that $R_{1\rho}$ relaxation was only sensitive to changes in pH while showing little to no sensitivity to glucose and lysine concentrations within the physiological range. Furthermore, the two-pool proton exchange modeling showed that this pH sensitivity was likely the result of amide proton exchange rates and not due to amine and hydroxyl exchange. $R_{1\rho}$ relaxation showed the greatest sensitivity to pH near body temperature as compared to R_2 and R_1 relaxation rates. Finally, the results of this work were in good agreement with the work by Spear and Gore, which also found that pH and temperature were two of the primary contributing factors to changes in proton exchange[29]. This work did extend the findings of Spear and Gore by using a more heterogenous protein media for the phantoms, a lower MR field strength, and a broader temperature range.

In the present study, a direct relationship between $R_{1\rho}$ relaxation rates and pH was observed between 6.0–7.0 at all spin-lock amplitudes (4.7 to 18.8 μT) used. This relationship was stronger as the spin-lock amplitude increased and appeared to be reaching a plateau at 18.8μT. The higher spin-lock amplitudes (14.1 and 18.8μT) showed sensitivity to pH up to 7.5, which were not evident at the lower spin-lock amplitudes. We restricted the maximum spin-lock amplitude to value consistent with clinical SAR limitations while maintaining maximum spin-lock duration of 100ms. These findings are in good agreement with previous studies reported in the literature (Table 2)[17,22,30,38–40]. A similar relationship between $R_{1\rho}$ relaxation rates and pH has been observed with spin-lock amplitudes greater than 25μT (1065Hz)[39], but the greatest pH sensitivity were observed when the spin-lock amplitude was

less than 23.5μT (1000Hz)[40] by Kettunen *et al.* as well as Spear and Gore[29]. Magnotta et al. previously reported a similar relationship between $R_{1\rho}$ and pH in agar phantoms, which contained potassium phosphate buffer (KPB) and bovine serum albumin (BSA) at 3T[30]. The only difference between the results presented here and by Magnotta et al.[30] was the wider range of the $R_{1\rho}$ sensitivity to pH likely due to differences in the proteins used for the phantom construction (BSA versus egg white ovalbumin). Finally, Willumsen observed exchange rate changes in the pH range 6.5–7.5 in aqueous ovalbumin media using deuterium experiments[41].

$R_{1\rho}$ showed little sensitivity to glucose and lysine in the presence of protein in the current study. In addition, no significant changes were observed in R_2 and R_1 relaxation rates. These findings contrast with previous work by Schuenke *et al.*[42] and Jin and Kim[17] conducted at ultra-high field. Both studies found a relationship between $R_{1\rho}$ relaxation rates and hydroxyl concentrations by adjusting glucose levels while the work by Jin and Kim also found a relationship with amine group concentrations by adjusting glutamate levels. A possible explanation for the insensitivity to hydroxyl concentration changes in the current study may be due to the different field strengths employed across the studies. The strength of the main magnetic field affects the chemical shift of the solute protons. The chemical shift for the hydroxyl group hydrogen is close to water (approximately 100Hz at 3T) and higher field strengths will increase the chemical shift and thus the ability to differentiate these two pools. Thus, the sensitivity to proton exchange is dependent on the strength of the static field; the current study employed a 3T scanner, which is more than 2.5 times lower than the previous field strengths used. The effect of spin-lock amplitude on sensitivity to hydroxyl concentration changes was studied by Spear and Gore[29]. Between spin-lock amplitudes of 200 to 800Hz, the authors showed a 40% increase in $R_{1\rho}$ when the concentration of glucose was increased from 0 to 50mM. We were unable to detect this much change in $R_{1\rho}$ signal. The decrease in SNR from spin-lock amplitude may have contributed to the lack of detection. Furthermore, a likely explanation for the $R_{1\rho}$ insensitivity to changes in amine group concentrations in the current study is the low amplitude spin-lock pulses. Amine protons exchange at rates faster than that of amide protons and require higher spin-lock amplitudes for sensitivity than were achievable at 3T while adhering to FDA limits for subject heating.

The Two-Pool model based on Cobb et al.[33] for proton exchange suggests that the sensitivity of $R_{1\rho}$ in these experiments to pH at spin-lock amplitudes available when performing human imaging studies (less than 23.5μT) is likely due to changes in amide exchange. The resulting model fit to the dispersion data was statistically significant and the resulting estimated parameters for R_2 exhibited similar trends as observed in our imaging experiments. Furthermore, the model fit using hydroxyl, and amine exchange parameters did not generate reasonable estimates for the relaxation measurements. It should be noted that the resulting model fit did not change significantly based on the initial values assigned to r_b, R_2, and $R_{1\rho}^{\infty}$. The calculated values for $R_{1\rho}^{\infty}$ were significantly shorter than the observed R_1 values. This indicates that additional factors may need to be added to the two-pool model to fully characterize the relaxation behavior. Finally, no changes in protein structure were observed based on the circular dichroism experiments.

In addition to $R_{1\rho}$ sensitivity to pH, R_2 and R_1 relaxation also showed sensitivity to pH as summarized in Table 2. The R_2 relaxation measurements conducted in this study showed sensitivity to pH. This work agrees with prior studies, which have shown similar R_2 sensitivity to pH[35,43,44]. Meiboom et al. attributed the pH sensitivity of R_2 relaxation rates to the breaking and forming of hydrogen bonds[43]. In addition, we observed the greatest R2 sensitivity to pH at 9 °C which agrees with work by Chopra *et al.*[35] R_1 relaxation rates also exhibited a dependence on pH at 9°C and 34°C with little change at 22°C in the range of pH 6.0–7.0. The literature has reported mixed results related to R_1 sensitivity to pH with some prior studies reporting pH sensitivity[39,45] while others finding no pH sensitivity[43,45]. These discrepancies may be related to the protein used, the ionic strength of the solutions in these experiments, the temperature, or pH range over which the measurements were made.

The results of this study suggest that changes in $R_{1\rho}$ relaxation rates that have been previously observed in various psychiatric and neurological disorders using spin-lock amplitudes of less than 23.5μT (1000Hz) may be due to changes in pH. Furthermore, we have previously shown a $500s^{-1}$ increase in the $R_{1\rho}$ relaxation rate in bipolar disorder as compared to controls[8]. Based on the results obtained at 34°C in this study, this magnitude of a $R_{1\rho}$ relaxation time change cannot be explained by hydroxyl and amine proton exchange based on the phantoms and modeling used in this study.

The pH, glucose and lysine concentration ranges tested here are broader than those occurring in brain tissue. However, there are limitations that need to be considered when extrapolating results from this phantom study to imaging of the brain *in vivo*. In egg white, there are two other proteins (ovotransferrin and ovomucoid) in solution apart from ovalbumin that exist in relatively large concentrations. The average acid dissociation constants (*i.e.* isoelectric point) of these proteins do not vary greatly (between 4–6). However, the brain expresses on the order of 15,000 proteins[46], with a range of isoelectric points. Different isoelectric points are likely to alter the relative pH sensitivity $R_{1\rho}$ relaxation rate. Differences in temperature before and after scanning were minimized due to the re-circulator; however, temperature did drift slightly during the experiment. While this temperature change was limited to approximately 2° C, it may have added to some of the variations in the relaxation measurements observed in the phantoms. In biological tissue, however, proton exchange is not the only contributor to R1ρ change. Diffusion of protons through regions where magnetic susceptibility change have also been shown to affect $R_{1\rho}$ considerably independent of proton exchange[47,48]. Though this work was conducted at 7T, the effects of magnetic susceptibility are relevant at all static field strengths. Recently, Ali *et al.* have concluded that the sensitivity of $R_{1\rho}$ to macromolecular change is significant and thus must be considered [49]. Due to pathophysiology, cellular density and metabolism will lead to changes in macromolecular concentration, which may also influence R1ρ relaxation times.

In conclusion, $R_{1\rho}$ is more sensitive to physiological changes in pH than glucose or lysine concentration in a protein at 3T. Near physiologic temperature, $R_{1\rho}$ is more sensitive to pH changes in the physiologic range than R_2 and R_1, although R_2 and R_1 also show some sensitivity to pH changes. $R_{1\rho}$ results also reflected the pH dependence of exchange in proteins. This suggests that changes in acidity in the presence of proteins may be an

underlying physiologic response driving the changes in $R_{1\rho}$ observed in applications to neurologic or psychiatric disorders at 3T. Additionally, we show that spin-lock pulses at low amplitudes produce adequate contrast to see pH related changes in tissue, well below SAR limits.

Supplementary Material

Refer to Web version on PubMed Central for supplementary material.

ACKNOWLEDGEMENTS

This work was supported by the National Institute of Mental Health (5R01MH11157802) and that of Biomedical Imaging and Bioengineering (5R01EB02201902).

ABBREVIATIONS

R_1	Longitudinal relaxation rate in the laboratory frame
R_2	Transverse relaxation rate in the laboratory frame
$R_{1\rho}(\omega)$	Longitudinal relaxation rate in the rotating frame
$T_{1\rho}$	$1/R_{1\rho}$
TSL	Duration of the spin-lock pulse block
CEST	Chemical exchange saturation transfer
B_0	Static magnetic field
B_1	Magnetic component of the radiofrequency field
SAR	Specific absorption
Glc	Glucose
Glu	Glutamate
HCl	Hydrochloric acid
NaOH	Sodium hydroxide
BSA	Bovine serum albumin
k_{ex}	Proton exchange rate

REFERENCE

1. Bai Y, Milne JS, Mayne L & Englander SW Primary structure effects on peptide group hydrogen exchange. Proteins 17, 75–86 (1993). [PubMed: 8234246]
2. Haris M, McArdle E, Fenty M, Singh A, Davatzikos C, Trojanowski JQ, Melhem ER, Clark CM & Borthakur A Early marker for Alzheimer's disease: hippocampus T1rho (T(1rho)) estimation. J Magn Reson Imaging 29, 1008–1012 (2009). [PubMed: 19388096]

3. Haris M, Singh A, Cai K, Nath K, Crescenzi R, Kogan F, Hariharan H & Reddy R MICEST: a potential tool for non-invasive detection of molecular changes in Alzheimer's disease. J. Neurosci. Methods 212, 87–93 (2013). [PubMed: 23041110]
4. Haris M, Nath K, Cai K, Singh A, Crescenzi R, Kogan F, Verma G, Reddy S, Hariharan H, Melhem ER & Reddy R Imaging of Glutamate Neurotransmitter Alterations in Alzheimer's Disease. NMR in biomedicine 26, 386 (2013). [PubMed: 23045158]
5. Haris M, Singh A, Cai K, Davatzikos C, Trojanowski JQ, Melhem ER, Clark CM & Borthakur A T1rho (T1ρ) MR imaging in Alzheimer' disease and Parkinson's disease with and without dementia. J Neurol 258, 380–385 (2010). [PubMed: 20924593]
6. Wassef SN, Wemmie J, Johnson CP, Johnson H, Paulsen JS, Long JD & Magnotta VA T1ρ imaging in premanifest Huntington disease reveals changes associated with disease progression. Mov. Disord (2015). doi:10.1002/mds.26203
7. Magnotta VA, Johnson CP, Follmer R & Wemmie JA Functional t1ρ imaging in panic disorder. Biol. Psychiatry 75, 884–891 (2014). [PubMed: 24157339]
8. Johnson CP, Follmer RL, Oguz I, Warren LA, Fiedorowicz JG, Magnotta VA & Wemmie JA Brain abnormalities in bipolar disorder detected by quantitative T1ρ mapping. Mol. Psychiatry 20, 201–206 (2015). [PubMed: 25560762]
9. Johnson CP, Christensen GE, Fiedorowicz JG, Mani M, Shaffer JJ, Magnotta VA & Wemmie JA Alterations of the cerebellum and basal ganglia in bipolar disorder mood states detected by quantitative T1ρ mapping. Bipolar Disorders 20, 381–390 (2018). [PubMed: 29316081]
10. Sepponen RE, Pohjonen JA, Sipponen JT & Tanttu JI A method for T1 rho imaging. J Comput Assist Tomogr 9, 1007–1011 (1985). [PubMed: 4056129]
11. Sepponen RE Imaging method. (1996).
12. Yuan J, Li Y, Zhao F, Chan Q, Ahuja AT & Wang Y-XJ Quantification of T 1ρ relaxation by using rotary echo spin-lock pulses in the presence of B 0 inhomogeneity. Phys. Med. Biol 57, 5003 (2012). [PubMed: 22805278]
13. Zu Z, Afzal A, Li H, Xie J & Gore JC Spin-lock imaging of early tissue pH changes in ischemic rat brain. NMR in Biomedicine 31, e3893 (2018). [PubMed: 29424463]
14. Brown RD & Koenig SH 1 /T1ρ and Low-Field 1 / T1 of Tissue Water Protons Arise from Magnetization Transfer to Macromolecular Solid-State Broadened Lines. Magn. Reson. Med 28, 145–152 (1992). [PubMed: 1331697]
15. Zong X, Wang P, Kim S-G & Jin T Sensitivity and Source of Amine-Proton Exchange and Amide-Proton Transfer Magnetic Resonance Imaging in Cerebral Ischemia. Magn. Reson. Med 71, 118–132 (2014). [PubMed: 23401310]
16. Jin T, Wang P, Zong X & Kim S-G Magnetic resonance imaging of the Amine–Proton EXchange (APEX) dependent contrast. NeuroImage 59, 1218–1227 (2012). [PubMed: 21871570]
17. Jin T & Kim S-G Characterization of non-hemodynamic functional signal measured by spin-lock fMRI. Neuroimage 78, 385–395 (2013). [PubMed: 23618601]
18. Duvvuri U, Poptani H, Feldman M, Nadal-Desbarats L, Gee MS, Lee WM, Reddy R, Leigh JS & Glickson JD Quantitative T1rho magnetic resonance imaging of RIF-1 tumors in vivo: detection of early response to cyclophosphamide therapy. Cancer Res. 61, 7747–7753 (2001). [PubMed: 11691788]
19. Gröhn OHJ, Kettunen MI, Mäkelä HI, Penttonen M, Pitkänen A, Lukkarinen JA & Kauppinen RA Early detection of irreversible cerebral ischemia in the rat using dispersion of the magnetic resonance imaging relaxation time, T1rho. J. Cereb. Blood Flow Metab 20, 1457–1466 (2000). [PubMed: 11043908]
20. Gilani IA & Sepponen R Quantitative rotating frame relaxometry methods in MRI. NMR Biomed. 29, 841–861 (2016). [PubMed: 27100142]
21. Jin T, Mehrens H, Hendrich KS & Kim S-G Mapping brain glucose uptake with chemical exchange-sensitive spin-lock magnetic resonance imaging. J. Cereb. Blood Flow Metab 34, 1402–1410 (2014). [PubMed: 24865996]
22. Kettunen MI, Gröhn OHJ, Silvennoinen MJ, Penttonen M & Kauppinen RA Effects of intracellular pH, blood, and tissue oxygen tension on T1rho relaxation in rat brain. Magn Reson Med 48, 470–477 (2002). [PubMed: 12210911]

23. Peng ZY, Simplaceanu V, Lowe IJ & Ho C Rotating-frame relaxation studies of slow motions in fluorinated phospholipid model membranes. Biophysical Journal 54, 81–95 (1988). [PubMed: 3416034]
24. Menon RS & Allen PS Solvent proton relaxation of aqueous solutions of the serum proteins alpha 2-macroglobulin, fibrinogen, and albumin. Biophysical Journal 57, 389–396 (1990). [PubMed: 1689591]
25. III, A. G. P., Fairbrother WJ, Cavanagh J, Skelton NJ & Rance M Protein NMR Spectroscopy, Second Edition: Principles and Practice. (Academic Press, 2006).
26. Knispel RR, Thompson RT & Pintar MM Dispersion of proton spin-lattice relaxation in tissues. Journal of Magnetic Resonance (1969) 14, 44–51 (1974).
27. Mäkelä HI, Vita ED, Gröhn OHJ, Kettunen MI, Kavec M, Lythgoe M, Garwood M, Ordidge R & Kauppinen RA B0 dependence of the on-resonance longitudinal relaxation time in the rotating frame (T1ρ) in protein phantoms and rat brain in vivo. Magnetic Resonance in Medicine 51, 4–8 (2004). [PubMed: 14705038]
28. Virta A, Komu M & Kormano M T1ρ of protein solutions at very low fields: Dependence on molecular weight, concentration, and structure. Magn. Reson. Med 37, 53–57 (1997). [PubMed: 8978632]
29. Spear JT & Gore JC New insights into rotating frame relaxation at high field. NMR Biomed. 29, 1258–1273 (2016). [PubMed: 26866422]
30. Magnotta VA, Heo H-Y, Dlouhy BJ, Dahdaleh NS, Follmer RL, Thedens DR, Welsh MJ & Wemmie JA Detecting activity-evoked pH changes in human brain. Proc. Natl. Acad. Sci. U.S.A 109, 8270–8273 (2012). [PubMed: 22566645]
31. Johnson CP, Thedens DR & Magnotta VA Precision-guided sampling schedules for efficient T1ρ mapping. J Magn Reson Imaging 41, 242–250 (2015). [PubMed: 24474423]
32. Greenfield NJ Using circular dichroism spectra to estimate protein secondary structure. Nature Protocols 1, 2876–2890 (2006). [PubMed: 17406547]
33. Cobb JG Quantitave Proton Relaxation in the Rotating Frame With Magnetic Resonance Imaging. (Vanderbilt University, 2011).
34. Cobb JG, Xie J & Gore JC Contributions of chemical and diffusive exchange to T1ρ dispersion. Magnetic Resonance in Medicine 69, 1357–1366 (2013). [PubMed: 22791589]
35. Chopra S, McClung RED & Jordan RB Rotating-frame relaxation rates of solvent molecules in solutions of paramagnetic ions undergoing solvent exchange. Journal of Magnetic Resonance (1969) 59, 361–372 (1984).
36. van Zijl PCM & Yadav NN Chemical exchange saturation transfer (CEST): what is in a name and what isn't? Magn Reson Med 65, 927–948 (2011). [PubMed: 21337419]
37. Sykes BD, Hull WE & Snyder GH Experimental evidence for the role of cross-relaxation in proton nuclear magnetic resonance spin lattice relaxation time measurements in proteins. Biophys J 21, 137–146 (1978). [PubMed: 623862]
38. Jokivarsi KT, Hiltunen Y, Gröhn H, Tuunanen P, Gröhn OHJ & Kauppinen RA Estimation of the onset time of cerebral ischemia using T1rho and T2 MRI in rats. Stroke 41, 2335–2340 (2010). [PubMed: 20814006]
39. Mäkelä HI, Gröhn OHJ, Kettunen MI & Kauppinen RA Proton Exchange as a Relaxation Mechanism for T1 in the Rotating Frame in Native and Immobilized Protein Solutions. Biochemical and Biophysical Research Communications 289, 813–818 (2001). [PubMed: 11735118]
40. Kettunen MI, Sierra A, Närväinen MJ, Valonen PK, Ylä-Herttuala S, Kauppinen RA & Gröhn OHJ Low Spin-Lock Field T1 Relaxation in the Rotating Frame as a Sensitive MR Imaging Marker for Gene Therapy Treatment Response in Rat Glioma. Radiology 243, 796–803 (2007). [PubMed: 17517934]
41. Willumsen L Hydrogen-deuterium exchange in ovalbumin. C R Trav Lab Carlsberg 36, 247–263 (1967). [PubMed: 5583459]
42. Schuenke P, Koehler C, Korzowski A, Windschuh J, Bachert P, Ladd ME, Mundiyanapurath S, Paech D, Bickelhaupt S, Bonekamp D, Schlemmer H-P, Radbruch A & Zaiss M Adiabatically

prepared spin-lock approach for T1ρ-based dynamic glucose enhanced MRI at ultrahigh fields. Magn. Reson. Med 78, 215–225 (2016). [PubMed: 27521026]

43. Meiboom S, Luz Z & Gill D Proton Relaxation in Water. The Journal of Chemical Physics 27, 1411–1412 (1957).
44. Schilling A, Blankenburg F, Bernarding J, Heidenreich J & Wolf K Intracerebral pH affects the T2 relaxation time of brain tissue. Neuroradiology 44, 968–972 (2002). [PubMed: 12483440]
45. Koenig SH & Schillinger WE Nuclear Magnetic Relaxation Dispersion in Protein Solutions I. APOTRANSFERRIN. J. Biol. Chem 244, 3283–3289 (1969). [PubMed: 5792660]
46. The human proteome in brain - The Human Protein Atlas. Available at: https://www.proteinatlas.org/humanproteome/brain (Accessed: 18th May 2018)
47. Spear JT, Zu Z & Gore JC Dispersion of relaxation rates in the rotating frame under the action of spin-locking pulses and diffusion in inhomogeneous magnetic fields: Dispersion of Relaxation Rates in the Rotating Frame. Magnetic Resonance in Medicine 71, 1906–1911 (2014). [PubMed: 23804212]
48. Spear JT & Gore JC Effects of diffusion in magnetically inhomogeneous media on rotating frame spin–lattice relaxation. Journal of Magnetic Resonance 249, 80–87 (2014). [PubMed: 25462950]
49. Ali SO, Fessas P, Kaggie JD, Zaccagna F, Houston G, Reid S, Graves MJ & Gallagher FA Evaluation of the sensitivity of R1ρ MRI to pH and macromolecular density. Magn Reson Imaging 58, 156–161 (2019). [PubMed: 30771445]

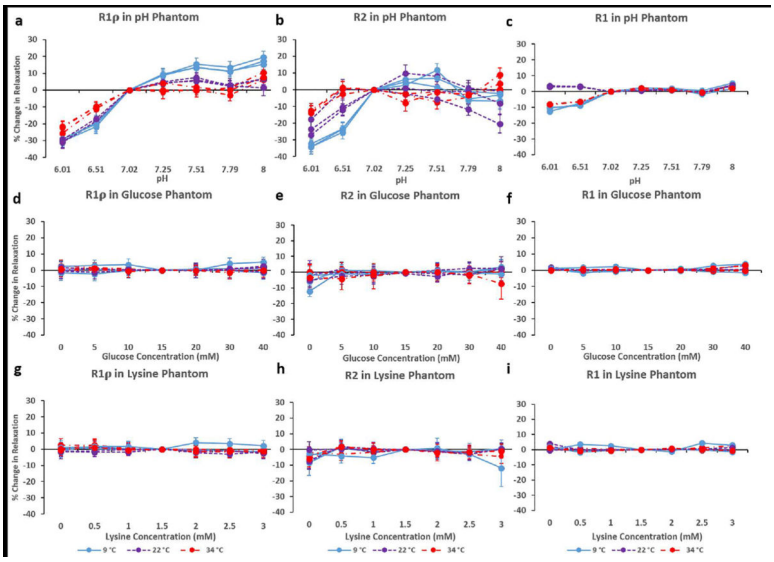

Figure 1.

Along the columns, change in $R_{1\rho}$ and R_2 and R_1 values are shown for the pH (a,b,c), glucose (d,e,f), and lysine (g,h,i) phantoms respectively, Measurements were obtained at three temperatures (9, 22, and 34 °C) and three independent measurements were obtained for each condition and relaxation parameter. Data for 9 °C is shown as a solid line (light blue), 22 °C is a dashed line (purple), and 34 °C is a dot/dashed line (red).

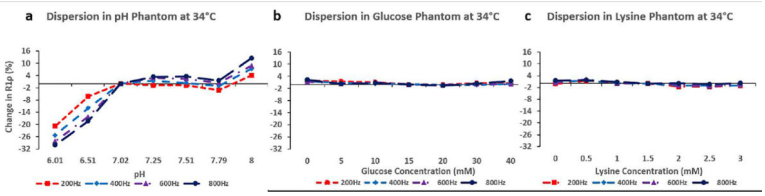

Figure 2.

Plots of relative change in $R_{1\rho}$ at 34 °C with varying spin-lock frequency (dispersion). R1ρ dispersion is shown for the pH (a), glucose (b) and lysine (c) phantoms.

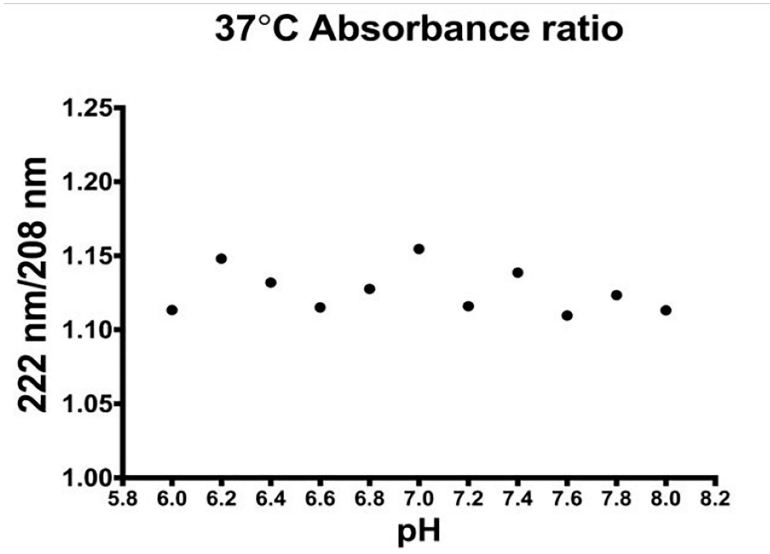

Figure 3.

Results from the circular dichroism experiment showing the ratio of absorbance between 222 and 208 nm wavelengths. The results show no change in the protein folding across the pH range studied.

Table 1:

Two-Pool model estimates for exchange rate (r_b), transverse relaxation rate (R_2), and $R_{1\rho}^{\infty}$. $R_{1\rho}$, R_1, and R_2 relaxation rates measured from the imaging experiments at 34°C are shown as well.

pH	Phantom $R_{1\rho}$ (s^{-1})* 800 Hz SL	Phantom R_1 (s^{-1})*	Model Fit $R_{1\rho}^{\infty}$ (s^{-1})*	Phantom R_2 (s^{-1})*	Model Fit R_2(s^{-1})*	Exchange Rate r_b (s^{-1})*
6.01	1.8±0.03	0.45±0.01	1.4±0.17	3.5±0.03	3.1±0.12	225±67
6.51	2.1 ±0.09	0.46±0.01	1.6±0.24	4.1±0.06	3.7±0.17	220±76
7.02	2.6±0.06	0.5±0.01	2.1±0.31	4.1±0.03	3.8±0.16	281±62
7.25	2.7±0.06	0.51±0.01	2.2±0.34	3.9±0.14	3.7±0.14	331±148
7.51	2.7±0.09	0.51±0.02	2.3±0.23	3.9±0.11	3.8±0.13	261±105
7.79	2.6±0.05	0.49±0.01	2.2±0.37	3.9±0.005	3.6±0.16	310±83
8	2.9±0.16	0.52±0.02	2.5±0.65	4.2±0.20	3.9±0.33	276±304

*Mean ± Standard Deviation

Table 2:

Relationship between amine, hydroxyl, and amine exchange and relaxation times from the literature spin-lock amplitudes (B_1) and static (B_0) field used in this study are included. The correlations are summarized in the table as positive (+), negative (−), or no correlation (↔). n/r signifies values not reported while empty cells were not measured in the study

Reference	Relaxation Trend with pH					
	$R_{1\rho}$	B_1 (μT)	R_2	R_1	pH Range	B_0 (T)
Kettunen *et al*.[22]	+	56.4	+		7.27–6.81 [a]	4.7
Magnotta *et al*.[30]	+	23.5			8.0–6.0 [b]	4.7
Jokivarsi *et al*.[38]	+	40	+		7.31-n/r [a]	4.7
Mäkelä *et al*.[39]	+	25.1–27.7	+	-	8.0–5.5	4.7
Jin *et al*.[17]	+	2.9–94			7.5–6.0	9.4
Koenig *et al*.[45]				-	5.2–4.0	0.1
				-	7.4–6.5	0.1
				+	10–8.4	0.1
Meiboom *et al*.[43]			+	↔	8–6	0.7
			-	↔	10–8	0.7
Schilling *et al*.[44]			+	↔	7–6	2.4
			-	↔	7–8	2.4
Owusu *et al*.	+	4.7–18.8	+	+	8.0–6.0	3.0
	Relaxation Trend with Hydroxyl Protons				**Concentration**	
Schuenke *et al*.[42]	+	5.0			5–20 mM	7.0
Jin *et al*.[17]	+	2.9–93.9			0–30 mM	9.4
Spear *et al*.[29]	+	1.2–235			0–200 mM	4.7,7.0
Owusu *et al*.	↔	4.7–18.8	↔	↔	0–40 mM	3.0
	Relaxation Trend with Amine Protons					
Jin *et al*.[17]	-	2.9–93.9			0–20 mM [b]	9.4
Owusu *et al*.	↔	4.7–18.8	↔	↔	0–3.0 mM	3.0

[a] in vivo data

[b] agarose phantom.